The Astrophysical Journal, 672:726–732, 2008 January 1
© 2008. The American Astronomical Society. All rights reserved. Printed in U.S.A.

X-RAY SIGNATURE OF CHARGE EXCHANGE IN THE SPECTRA OF L-SHELL IRON IONS

P. Beiersdorfer
Space Sciences Laboratory, University of California, Berkeley, CA 96720; and University of California Lawrence Livermore National Laboratory, Livermore, CA 94550; beiersdorfer@ssl.berkeley.edu

L. Schweikhard
Institut für Physik, Ernst-Moritz-Arndt Universität, D-17487 Greifswald, Germany

and

P. Liebisch[1] and G. V. Brown
University of California Lawrence Livermore National Laboratory, Livermore, CA 94550
Received 2007 January 8; accepted 2007 August 3

ABSTRACT

The X-ray signature of charge exchange between highly charged L-shell iron ions and neutral gas atoms was studied in the laboratory in order to assess its diagnostic utility. Significant differences with spectra formed by electron-impact excitation were observed. In particular, a strong enhancement was found of the emission corresponding to $n \geq 4 \rightarrow n = 2$ transitions relative to the $n = 3 \rightarrow n = 2$ emission. This enhancement was detectable even with relatively low-resolution X-ray instrumentation ($E/\Delta E \approx 10$) and may enable future identification of charge exchange as a line-formation mechanism in astrophysical spectra.

Subject headings: atomic data — atomic processes — line: formation — X-rays: general

Online material: color figures

1. INTRODUCTION

Ion-atom charge-exchange reactions gained new importance when recent satellite missions discovered X-ray emission from the interaction of solar-wind ions with gases in cometary comae (Lisse et al. 1996, 1999a, 1999b, 2001, 2005; Dennerl et al. 1997; Mumma et al. 1997; Ip & Chow 1997; Krasnopolsky et al. 1997, 2002; Krasnopolsky 1997; Neugebauer et al. 2000). Charge exchange involving heavy ions in the solar wind has been shown as the process most likely to explain this phenomenon. Ion-atom charge exchange is also believed to drive the X-ray emission from planetary atmospheres, including the geocorona, and to form much of the soft X-ray background in the heliosphere (Dennerl et al. 2006; Wargelin et al. 2004; Cravens 2002; Bhardwaj et al. 2007). The later has spurred observations to detect X-rays produced by charge exchange in astrospheres (Wargelin et al. 2001; Wargelin & Drake 2002). Such X-rays would manifest themselves as an X-ray halo around the parent star and would provide a measure of the star's mass-loss rate.

A laboratory simulation of cometary X-ray emission that involved the K-shell emission of helium-like and hydrogen-like carbon, nitrogen, and oxygen was highly successful in reproducing the observed X-ray emission from comet S4 Linear at spectral energies above 300 eV (Beiersdorfer et al. 2003b). Laboratory simulations that also included the K-shell emission of helium-like neon successfully described the emission from comet McNaught-Hartley (Beiersdorfer et al. 2005b). In addition, theoretical descriptions of K-shell X-ray emission from charge exchange (Kharchenko & Dalgarno 2001; Perez et al. 2001; Kharchenko et al. 2003; Otranto et al. 2006) have made much progress since the earliest simplified models, which consisted of either only a single X-ray line from a given ion (Häberli et al. 1997) or multiple lines with equal intensities (Wegmann et al. 1998; Schwadron & Cravens 2000).

Despite several recent laboratory measurements of the K-shell X-ray emission, spectral models still do not correctly reproduce all of the most telling features in K-shell spectra. For example, the intensity of the K-shell emission emanating from levels with high principal quantum number n or the emission from the helium-like $1s2s$ metastable level observed in the laboratory in low-energy collision systems (<100 eV amu^{-1}) are not readily reproduced by theory (Beiersdorfer et al. 2003b; Wargelin et al. 2005). All or part may be due to the fact that multiple electron capture is typically not yet modeled. Multiple electron capture has been shown to be important when the interaction gas is a many electron atom or molecule (Ali et al. 1994, 2005; Hasan et al. 2001). By contrast, good agreement was achieved between theoretical models and the recent observation of the K-shell X-ray emission of helium-like argon (Beiersdorfer et al. 2005a). This emission was produced in the interaction of hydrogen-like argon ions and atomic hydrogen. In this case, double or multiple electron capture could be ruled out, and the collision energy was high (40 keV amu^{-1}). However, in many solar system and astrophysical situations the ion-atom collision energy is considerably lower; solar-wind ions typically have speeds corresponding to several keV amu^{-1}, and their energy may drop to several tens of eV after traversing the bow shock of a comet (Wegmann et al. 1998). Thermal collision energies (few tens of eV amu^{-1}) are expected in the interaction of evaporating clouds of gas and shocked gas in supernova remnants (Wise & Sarazin 1989). Moreover, multielectron atoms and complex molecular gases are sure to play a role in charge-exchange reactions involving cometary and planetary atmospheres.

The X-ray emission from ions with an open L-shell is even less understood than that from ions with a K-shell vacancy. Laboratory X-ray spectra are essentially nonexistent. Measurements of L-shell lines have concentrated on relatively simple systems such as those in lithium-like or berylium-like ions of low-Z elements (carbon, nitrogen, and oxygen; Bliek et al. 1998; Lubinski et al. 2000; Ehrenreich et al. 2005). The corresponding lines are situated

[1] Current address: Biotronik GmbH & Co. KG, D-12359 Berlin, Germany.

in the extreme-ultraviolet corresponding to photon energies $\leq$100 eV. These systems are close analogs to the hydrogen-like and helium-like ions. However, additional lines appear in these spectra because of the fact that the $n = 2$ ground configuration may assume both an $l = 0$ and $l = 1$ angular momentum state. In these low-Z low-charge ions electron capture is mainly to the $n = 3, 4$ levels, and the L-shell emission is totally dominated by transitions from $n = 3$ or $n = 4$ to $n = 2$. In order to model X-ray spectra produced by charge exchange that may play a role in astrophysics and the solar system, it is necessary to study higher Z ions. For example, charge exchange involving the L-shell ions of sulfur may be responsible, at least in part, for the X-ray emission observed with *Chandra* in the Jovian aurora (Cravens et al. 2003; Gladstone et al. 2002; Elsner et al. 2005). The only measurements of the X-ray emission of a high-Z L-shell ion we are aware of is that of krypton ions performed at the electron beam ion source at the Macdonald Laboratory at the Kansas State University (Tawara et al. 2002) and subsequently at the electron beam ion trap at the National Institute of Standards and Technology (Tawara et al. 2003). These measurements were carried out at rather high electron-ion interaction energies.

In what follows, we present measurements of the L-shell X-ray emission produced by charge exchange involving highly charged iron ions, Fe^{18+}–Fe^{24+}. The collision energies are at the thermal ion temperature, which are estimated at around 10–20 eV amu^{-1}. Such iron ions may play a role, for example, in extrasolar systems with stellar winds hotter than those of our Sun. Moreover, our measurements may be considered a first step toward understanding the L-shell emission from highly charged sulfur ions undergoing charge exchange processes in the Jovian atmosphere, as many of them are likely to be in a similar isoelectronic configuration (fluorine-like though helium-like) as the iron ions studied here.

The charge of the iron ions ($q \leq 24$) is such that capture proceeds to levels with $n \approx 9, 10$ (Janev & Winter 1985). We can distinguish the more energetic emission that proceeds from these high-n levels to the $n = 2$ ground level and softer X-rays that result from an $n = 3 \rightarrow n = 2$ transition even with a relatively low-resolution spectrometer. We also distinguish those X-rays that result from an $n = 4 \rightarrow n = 2$ or $n = 5 \rightarrow n = 2$ transition. The ratio of the two types of X-rays, i.e., the ratio of those X-rays emanating from levels higher than $n = 3$ to those emanating from $n = 3$, was dubbed the hardness ratio $\mathcal{H}$ (Beiersdorfer et al. 2000a). It plays an important diagnostic role in the interpretation of K-shell X-ray spectra from hydrogen-like ions (Beiersdorfer et al. 2001; Perez et al. 2001; Wargelin et al. 2005; Otranto et al. 2006). Our present measurements show that the hardness ratio is also an important diagnostic in L-shell X-ray spectra involving thermal ions. We show that it is several times larger than the hardness ratio observed when the emission is produced by electron-impact excitation. We find that the main contribution to the overall X-ray emission comes from $n = 4 \rightarrow n = 2$ and $n = 5 \rightarrow n = 2$ transitions. As we show, the enhancement of the emission from $n \geq 4$ levels can be observed with low-resolution solid-state detectors, making this a robust indicator for charge exchange.

2. EXPERIMENTAL SETUP AND PROCEDURE

Charge-exchange studies on the Livermore EBIT-I, EBIT-II, and SuperEBIT electron beam ion traps have employed the magnetic (trapping) mode (Beiersdorfer et al. 1995a, 1996a, 1996c; Schweikhard et al. 1995, 2002). These studies have considered the K-shell X-ray production by low-energy charge-exchange collisions and involved ions with charge as low as C^{5+} and as high as U^{91+} (Beiersdorfer et al. 2000a, 2001, 2003b, 2005c; Schweikhard et al. 1998). The magnetic mode has also been used extensively

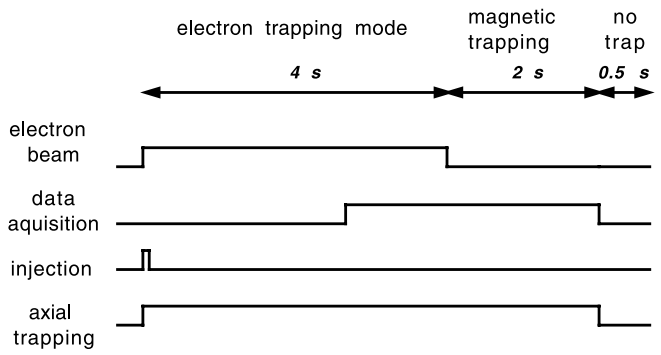

FIG. 1.—Experimental timing sequence.

for measurements of radiative transition rates of metastable levels in highly charged ions (Beiersdorfer et al. 1996c, 2003a; Schweikhard et al. 2002; Crespo López-Urrutia et al. 1998; Neill et al. 2000; Träbert et al. 2000, 2001, 2002; Lapierre et al. 2005). The latter measurements have shown that the emission from long-lived metastable levels can readily be observed. In other words, the radiative decay time of these metastable levels (typically tens of milliseconds or less) is orders of magnitude shorter than the trapping time of the ions in the magnetic trap (typically on the order of seconds). This is in contrast to measurements using ions extracted from a source and moving at high velocities. Here, the decay of metastable levels takes place outside the detection region and cannot be observed (Ali et al. 2005; Tawara et al. 2002, 2003; Greenwood et al. 2000, 2001). In what follows, we use the magnetic mode for measuring the iron L-shell emission.

We employ the timing sequence shown in Figure 1 to switch from the so-called electron mode, which is the usual operating mode of an electron beam ion trap, to the magnetic mode. After injection from a metal vapor vacuum arc source (Brown et al. 1986), the iron ions are ionized by the electron beam during the electron mode. While the electron beam is on, X-rays are mainly produced by electron-impact excitation. However, there is also some contribution from bremsstrahlung and radiative recombination. The latter emission produces X-rays with energy higher than the electron beam energy, because the energy liberated in radiative electron capture equals the energy of the free electron, i.e., the beam energy, plus the ionization potential of the recombined ion. Spectra obtained during the electron mode of operation are shown in Figures 2 and 3. The spectra were taken with a Kevex SiLi solid-state detector providing an energy resolving power of $E/\Delta E \approx 10$ over a broad energy range.

In the magnetic mode, the electron beam ion trap is operated without the electron beam. In this case, the electron beam ion trap operates like a Penning trap, i.e., the ions are confined radially by a strong (3 T) magnetic field and axially by a static electric field which creates a potential well in the direction of the magnetic field lines (Major et al. 2004). The trap is switched to the magnetic mode of operation after 4 s. This time suffices to optimize the abundance of the ions of interest, but is short enough to prevent the accumulation of high-Z impurity ions from elements such as barium or tungsten. Because in the magnetic mode there is no electron beam to excite the ions, X-ray production is by charge exchange only. Spectra obtained during the magnetic mode of operation are shown in Figures 2 and 3. The duration of the magnetic mode is 2 s.

After the magnetic mode, the trap is opened to purge it of the iron ions and of background ions which may have accumulated, as indicated in Figure 1. The axial potential well is switched off by dropping the voltage of the top drift tube (typically 100 or 200 V)

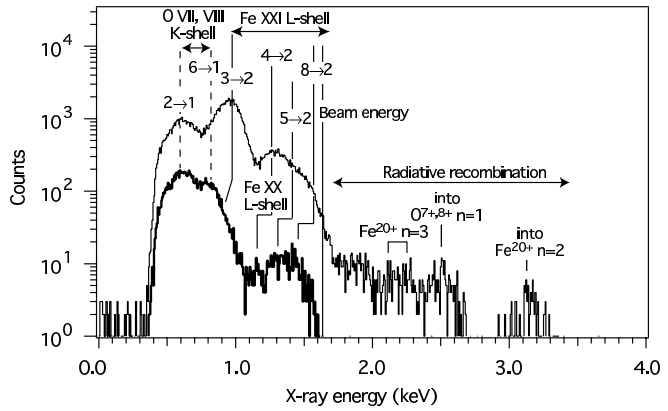

FIG. 2.—X-ray spectra in the electron trapping mode and the magnetic trapping mode at a drift tube voltage of $V_{DT} = 1.65$ kV. Energies of the iron L-shell transitions are shifted in the magnetic mode spectra indicating that the emitting ion has one charge less than in the corresponding ion in the electron trapping mode.

to zero. Then a new injection takes place, and a new ionization cycle is started.

Our measurements employed beam energies in the range of 1.10 and 2.45 keV. These energies were chosen to produce the relevant open L-shell iron ions. A summary of the minimum electron energy needed to ionize a given ion to the next charge state is given in Table 1.

The spectra shown in Figures 2 and 3 were produced at electron beam energies of 1.65 and 1.85 keV, respectively. At these energies iron may ionize to Fe^{20+} and Fe^{22+}, respectively, because the ionization potential of Fe^{19+} is 1.582 keV, while that of Fe^{20+} is 1.689 keV. Therefore, a beam energy of 1.65 keV is high enough to ionize Fe^{19+}, but it is too low to ionize Fe^{20+}. Similarly, the ionization potential of Fe^{21+} is 1.799 keV, while that of Fe^{22+} is 1.950 keV. Therefore, a beam energy of 1.85 keV enables the production of Fe^{22+} but not that of iron ions with higher charge. The beam energy only determines the maximum charge state that can be produced. Lower ionization stages may also be present. However, the maximum possible charge state along with the next highest charge state typically dominate the charge balance, as shown in earlier measurements (Brown et al. 2002) and corresponding ionization calculations (Beiersdorfer et al. 2000b; Beiersdorfer 2003, illustrated in Fig. 4).

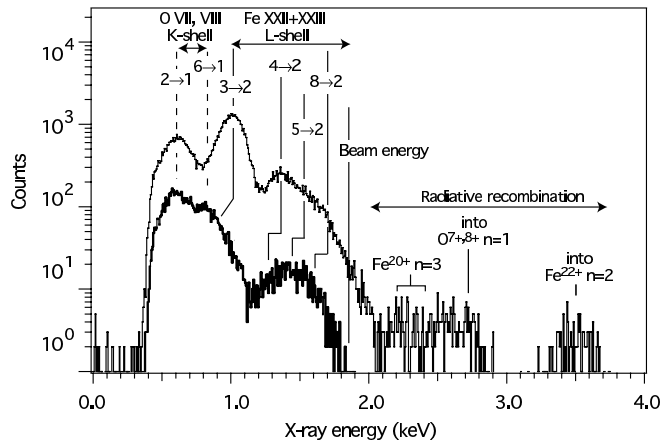

FIG. 3.—X-ray spectra in the electron trapping mode and the magnetic trapping mode at a drift tube voltage of $V_{DT} = 1.85$ kV. Energies of the iron L-shell transitions are shifted in the magnetic mode spectra indicating that the emitting ion has one charge less than in the corresponding ion in the electron trapping mode.

TABLE 1
IONIZATION ENERGIES AND MAIN X-RAY FEATURES OF L-SHELL IRON IONS

Charge State	Isoelectronic Sequence	E_{min}[a] (keV)	E_{ave}[b] (keV)	E_{2-4}[c] (keV)	Series Limit[d] (keV)
Fe^{16+}	Ne-like	0.489	0.771	1.011	1.262
Fe^{17+}	F-like	1.26	0.794	1.084	1.358
Fe^{18+}	O-like	1.36	0.842	1.176	1.456
Fe^{19+}	N-like	1.46	0.966	1.240	1.582
Fe^{20+}	C-like	1.58	1.009	1.290	1.689
Fe^{21+}	B-like	1.69	1.023	1.380	1.799
Fe^{22+}	Be-like	1.80	1.046	1.425	1.950
Fe^{23+}	Li-like	1.95	1.109	1.520	2.046

[a] Minimum energy needed to produce a given ion based on calculations by J. H. Scofield (private communication).
[b] Average energy of the strongest $n = 3 \rightarrow n = 2$ transitions based on measurements by Brown et al. (2002) and Beiersdorfer et al. (2004).
[c] Average energy of strongest $n = 4 \rightarrow n = 2$ based on measurements by Chen et al. (2007).
[d] Values from Kelly (1987).

From previous measurements (Beiersdorfer et al. 1995b, 1995c, 1996b) and related simulations (Liebisch 1998) the temperature of the trapped iron ions in the axial potential well of $V_{ax} = 200$ V can be estimated to be about 500 eV. If we assume that the energy of the ions remains the same after the beam is turned off, this means the collision energy distribution is about 10 eV amu^{-1}. There is some evidence that the ion energy drops after the beam is turned off, and the actual average collision energy may be lower than this value. The present measurement thus provides X-ray data for the lower end of the collision-energy scale typical for laboratory measurements.

3. RESULTS

3.1. *Collisional Spectra*

The spectra from the electron trapping mode are dominated by the iron L-shell emission from the $n = 3 \rightarrow n = 2$ transitions. At 1.65 keV beam energy, this peak is observed roughly at 990 eV. In the case of the 1.85 keV measurement, the peak is slightly shifted to 1025 eV. Emission from the iron $n = 4 \rightarrow n = 2$ transitions is seen at 1290 and 1380 eV, respectively, in the two measurements. These values can be compared with the peak values of the $n = 3 \rightarrow n = 2$ and $n = 4 \rightarrow n = 2$ emission lines of the various charge states of iron summarized in Table 1. This table lists the intensity-averaged energy of line emission of the strongest lines observed in the electron beam ion trap by Brown et al. (2002) and Chen et al. (2007). In the case of the $n = 3 \rightarrow n = 2$ transitions of Fe XVII the intensity-averaged energy E_{ave} of the lines observed on the PLT tokamak by Beiersdorfer et al. (2004) were used. Looking at Table 1, the averaged values for the $n = 3 \rightarrow n = 2$ transitions in Fe XX and Fe XXI are 966 and 1009 eV, respectively. The observed value is between these two numbers, indicating that a charge balance dominated by these two charge states was attained at a beam energy of 1.65 keV. Similarly, the averaged values for the $n = 4 \rightarrow n = 2$ transitions in Fe XX and Fe XXI are 1240 and 1290 eV, respectively. The observed value in this case is at the higher of these two numbers, indicating a charge balance dominated by Fe XXI. The averaged values for the $n = 3 \rightarrow n = 2$ transitions in Fe XXII and Fe XXIII given in Table 1 are 1023 and 1046 eV, respectively. The observed value is close to the value for Fe XXII, indicating that the charge balance is dominated by this charge state at a beam energy of 1.85 keV. The averaged values for the $n = 4 \rightarrow n = 2$ transitions in Fe XXII and

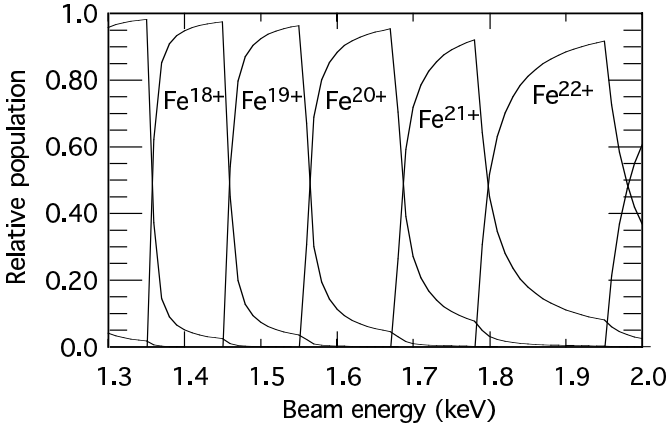

FIG. 4.—Calculated ionization balance as a function of electron beam energy.

Fe XXIII are 1380 and 1425 eV, respectively, and the observed value again matches the value for Fe XXII.

The electron trapping mode spectra in Figures 2 and 3 also show a strong peak near 600 eV. This peak is attributed to the $n = 2 \rightarrow n = 1$ oxygen K-shell emission from O^{7+} (and to a lesser extent, from O^{6+}). Emission from higher members of the O^{7+} Lyman series undoubtedly contributes to the spectra as well, but cannot be resolved from the $n = 3 \rightarrow n = 2$ iron emission. The oxygen emission is due to background ions in the trap, as discussed in more detail below.

The energy discriminator in the pulse height analysis system associated with the SiLi detector prohibited recording X-rays with energy below about 400 eV. This setting was chosen to match the detection efficiency of the SiLi detector. The quantum efficiency of the SiLi detector is greatly reduced for X-rays with energies below that value because of a thin proprietary Be window needed to block visible light from hitting the detector.

In spectra observed during the electron mode of operation, iron L-shell emission from the higher n-levels can be seen all the way to the energy of the electron beam or at the series limit of the highest charge state produced by the beam. X-rays are also detected at energies above the iron L-shell series limits for the respective beam energy of a given measurement. X-rays with energy above the series limit but below the energy of the electron beam are attributed to bremsstrahlung. Those with energy above that of the electron beam are due to radiative electron capture. For example, the X-rays near 3.15 keV in Figure 2 are produced by the capture of a 1.65 keV beam electron into the $n = 2$ shell of an Fe^{20+} ion. The emitted X-ray radiates away the sum of the 1.65 keV beam energy and the 1.50–1.55 keV binding energy of the $n = 2$ electron in Fe^{19+}. (The binding energy depends on the actual configuration into which the electron is captured.) The fact that most radiative recombination X-rays are close to 3.2 keV shows that Fe^{20+} dominates the ionization balance. X-rays produced by radiative electron capture into the $n = 2$ shell of an Fe^{19+} ion would have an energy 100 eV less, because its binding energy is on average about 100 eV less than that of Fe^{20+}, as seen from the data in Table 1. Those produced by radiative electron capture into the $n = 2$ shell of an Fe^{18+} ion, for example, would have an energy about 200 eV less. Some evidence for such capture is seen in the spectrum, although the signal is weak and in part may be due to the low energy resolution of the detector, which spreads the signal, especially when displayed on a logarithmic scale. The radiative recombination spectrum is typically a better indicator of the ionization balance in the trap than the (rather uncertain and unresolved) signal from the $n = 3 \rightarrow n = 2$ or $n = 4 \rightarrow n = 2$ transitions we discussed above.

Radiative electron capture into the $n = 3$ shell of an Fe^{20+} ion is situated at around 2.1–2.2 keV in the electron trapping mode spectra in Figure 2. No clear peak is seen at this location. Instead, we see a broad "background" of unresolved radiation recombination photons. This background is due not only to $n = 3$ capture by iron ions but is also caused by recombination X-rays due to electron capture by bare oxygen ions, the peak of which is situated near 2.52 keV, and possibly by bare nitrogen and carbon ions with corresponding peaks near 2.32 keV and 2.14 keV, respectively. Moreover, the peaks corresponding to capture by hydrogen-like oxygen, nitrogen, and carbon are at 2.39, 2.20, and 2.04 keV, respectively. The oxygen, and possibly nitrogen and carbon, ions are formed by ionizing residual background gases. We note that these residual gases provide the neutral partners for the charge transfer reactions with the iron ions in the magnetic mode.

The electron trapping mode spectrum in Figure 3 shows the same radiative recombination features as the spectrum in Figure 2, except that all energies are shifted by the increase in the beam energy. In addition, the recombination peak at 3.5 keV is noticeably broader than that at 3.2 keV in Figure 2. This broadening indicates that both Fe^{22+} and Fe^{21+} are present in the trap and capture beam electrons, in agreement with our earlier discussion of the $n = 3 \rightarrow n = 2$ and $n = 4 \rightarrow n = 2$ transitions.

3.2. *Charge-Exchange Spectra*

After the electron beam is turned off, radiative electron capture, bremsstrahlung, and electron-impact excitation cease. The spectral emission, therefore, is very different in the magnetic mode. All X-rays are now either emitted from metastable states populated in the electron trapping mode (Schweikhard et al. 2002) or are produced by charge exchange between the ions and the residual background gases in the trap. We can exclude X-rays from metastable levels, if we wait long enough, which typically means commencing data acquisition a few microseconds after the beam is turned off. Background gases for charge exchanging interactions in the present case are presumed to be the usual gases in a vacuum system, i.e., O_2, N_2, H_2O, and CO_2. The presence of these gases is indicated by the residual gas analyzer on our machine.

Another notable difference between the electron mode and magnetic mode spectra is the large reduction of the observed X-ray flux. This is in part due to the fact that a given ion will produce only a single X-ray when it undergoes charge exchange. The ion changes its charge state and thus is destroyed in the process. In contrast, a given ion can be excited over and over again in the electron trapping mode and can thus emit many X-rays. Moreover, the charge exchange process is rather slow with an e-folding time of seconds because of the low density of neutrals in the trap (Beiersdorfer et al. 1996c).

The magnetic-mode spectrum of Figure 2 gives the typical signature for charge transfer processes after turning off the electron beam. X-ray emission at energies above that of the electron beam has ceased, and no emission that can be ascribed to bremsstrahlung or radiative electron capture is seen. Moreover, the shape of the emission below the beam energy differs markedly from that recorded during the time when the beam was on.

Looking at the magnetic mode spectra in Figures 2 and 3 we do not see strong emission from high-n levels near $n_c \approx 8$–10. By contrast, we find strong $n = 5 \rightarrow n = 2$ emission. This emission is stronger or as strong as the emission corresponding to the

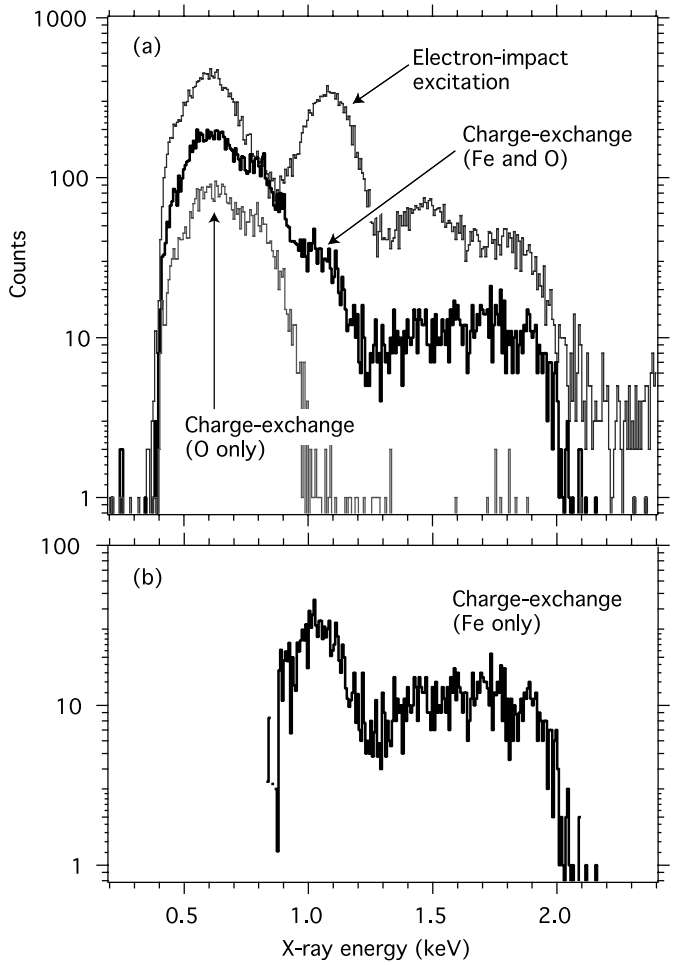

FIG. 5.—X-ray spectra in the electron trapping mode and the magnetic trapping mode at a drift tube voltage of $V_{DT} = 2.45$ kV. (*a*) Raw spectra obtained with and without iron injection; (*b*) iron spectrum after subtraction of oxygen emission. [*See the electronic edition of the Journal for a color version of this figure.*]

$n = 4 \rightarrow n = 2$ transitions. This is very different from the emission recorded during the time when the beam was on, when the $n = 5 \rightarrow n = 2$ emission is smaller than the $n = 4 \rightarrow n = 2$ emission. Moreover, the $n = 3 \rightarrow n = 2$ emission, which dominates in the electron mode spectrum, is reduced compared to the $n = 4 \rightarrow n = 2$ emission. In fact, the $n = 3 \rightarrow n = 2$ emission can no longer compete effectively with the emission from the oxygen peaks.

In order to isolate the $n = 3 \rightarrow n = 2$ iron emission, we must account for the K-shell oxygen emission. The process we use to do so is illustrated in Figure 5. The figure shows the electric and magnetic mode spectrum of iron obtained at a beam energy of 2450 eV. At this beam energy, most charge exchange X-ray emission comes from Fe XXIV produced by charge exchange involving Fe^{24+} ions. The contamination of the spectrum by K-shell oxygen is clearly seen both in the electric and magnetic mode spectrum. We have also recorded a background spectrum in the absence of iron injection, as shown in Figure 5*a*. We account for the oxygen contamination (and any other impurities, which may contribute to the background emission) by subtracting the measured background emission from the iron data. The resulting pure iron emission is shown in Figure 5*b*. Additional spectra produced after subtracting the background contamination are shown in Figure 6. The three panels in Figure 6 show emission dominated by Fe XX, Fe XXII, and Fe XXIII.

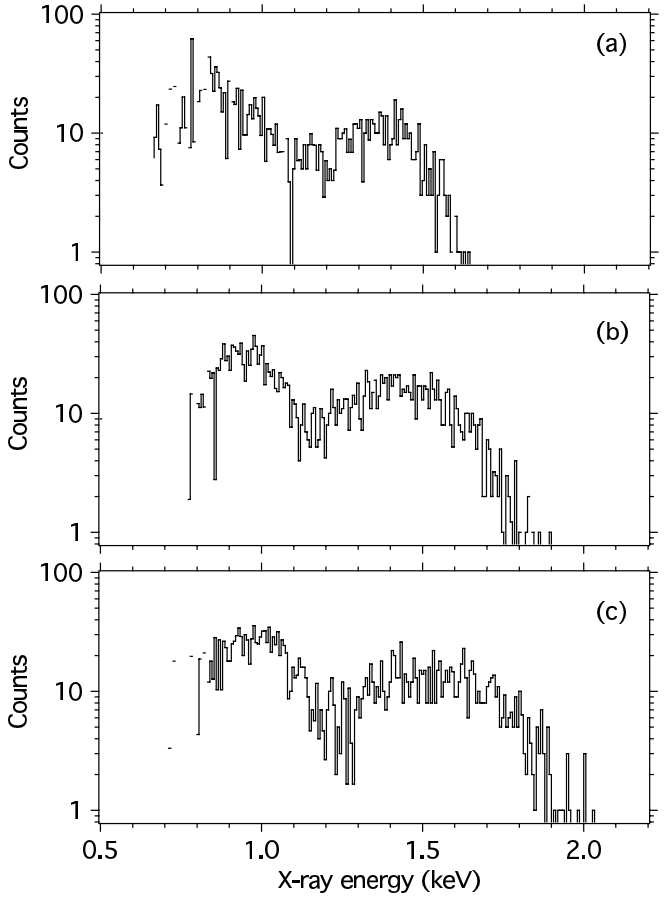

FIG. 6.—X-ray spectra of iron produced by charge-exchange in the magnetic trapping mode. The oxygen emission has been subtracted in each case; (*a*) $V_{DT} = 1.65$ kV (Fe XX); (*b*) $V_{DT} = 1.85$ kV (Fe XXII); (*c*) $V_{DT} = 2.15$ kV (Fe XXIII).

In Figure 7 we show the spectrum produced by charge exchange from Figure 3 after subtraction of the background emission and compare it to data produced by electron-impact excitation. The heights of the $n = 3 \rightarrow n = 2$ of both spectra are normalized to each other, and both spectra are shown on a linear scale. This

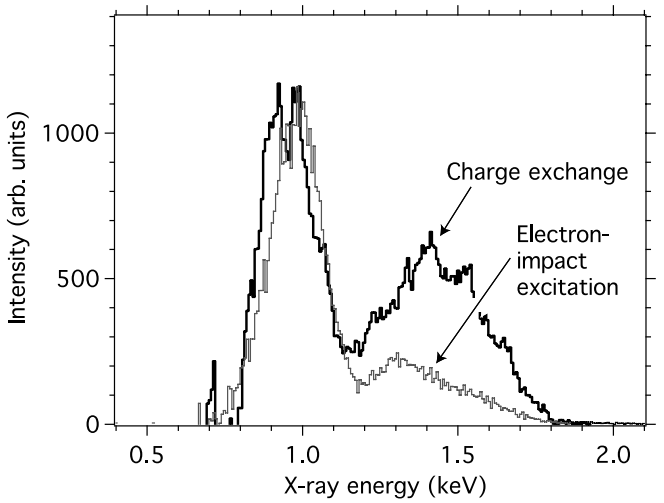

FIG. 7.—Comparison of X-ray spectra of iron produced by charge-exchange in the magnetic trapping mode at $V_{DT} = 1.85$ kV and by electron-impact excitation at $V_{DT} = 1.75$ kV. The oxygen emission has been subtracted in both cases. The heights of the $n = 3 \rightarrow n = 2$ emission of both spectra are normalized to each other. [*See the electronic edition of the Journal for a color version of this figure.*]

TABLE 2
Relative Iron X-Ray Intensities

Electron Beam Energy (keV)	$4 \rightarrow 2$	$5 \rightarrow 2$	$n_c \rightarrow 2$
Charge Exchange			
1.65	0.25	0.38	0.22
1.75	0.41	0.59	0.29
1.85	0.35	0.53	0.35
1.95	0.37	0.43	0.33
2.05	0.38	0.41	0.34
2.45	0.35	0.38	0.35
Electron-Impact Excitation			
Multiple	0.20	0.15	0.10

Notes.—Intensities are formed by charge exchange or electron-impact excitation at energies corresponding to $n \rightarrow 2$ decay and are expressed as a fraction of the intensity of the $n = 3 \rightarrow 2$ transition. Here, $n_c \approx 8, 9$ is the level into which the electron is most likely captured during charge exchange. The measurement uncertainties are less than 10%.

allows for better comparison of the relative magnitudes of the emission from levels with $n > 3$, and a strong enhancement is readily seen. The spectrum produced by electron-impact excitation was obtained at a beam energy of 1750 eV. This is 100 eV less than the corresponding spectrum produced by electron-impact excitation in Figure 3. The reason for this choice is that the charge balance of the emitting iron ions is roughly comparable for the two cases, as the emission produced by charge exchange always emanates from at least one charge state less than in the case of the emission produced by electron-impact excitation. Because the charge balance in the two spectra is only roughly the same, we cannot be sure that the shift in centroid energy toward lower energy of the $n = 3 \rightarrow n = 2$ emission for the charge exchange spectrum is significant. However, if it is, it would mean that charge exchange has a tendency to enhance the lower energy $3s \rightarrow 2p$ transitions over the higher energy $3d \rightarrow 2p$ transitions, which usually dominate the emission.

A quantitative summary of the relative emission from the $n = 4 \rightarrow n = 2$, $n = 5 \rightarrow n = 2$, and $n \approx 8, 9, 10 \rightarrow n = 2$ emission with respect to the $n = 3 \rightarrow n = 2$ emission is given in Table 2. The table lists the relative emission for iron excited by charge exchange as well as by electron-impact excitation. The relative intensities for the latter are within an uncertainty of 0.03 the same for all energies studied, and the values given are thus the averages for all energies.

The values in Table 2 show that charge exchange strongly enhances the relative emission from levels with $n \geq 4$. In particular, the $n = 4 \rightarrow n = 2$ emission is enhanced by about a factor of 2 over that observed if the iron ions are excited by electron-impact collisions. This enhancement grows to a factor of 4 for the $n = 5 \rightarrow n = 2$ emission. It ranges between factors of 2 and 4 for the $n_c \approx 8, 9 \rightarrow n = 2$ emission. This significant difference may enable future identification of charge exchange as a line formation mechanism in astrophysical spectra.

4. DISCUSSION AND SUMMARY

As we have shown, the L-shell X-ray emission from thermal $\leq$10–20 eV amu^{-1} iron ions interacting with neutral gases via charge exchange is significantly different from the emission produced by electron-impact excitation. The emission corresponding to $n \geq 4 \rightarrow n = 2$ transitions is greatly enhanced. This enhancement is by factors of 2–4 at the resolution of our detectors. The increase of the hardness ratio over that expected from electron-impact excitation thus is a diagnostic of the presence of charge exchange, similar to what was found in the case of the emission from hydrogen-like ions (Beiersdorfer et al. 2001).

In order to satisfy radiative selection rules, an electron captured into a level n_c can decay to the $n = 2$ ground state in Fe^{q+} with $q = 17$–22 only if its angular momentum value is either $l = 0$ or 2, as the ground state has only an $l = 1$ (p-state) vacancy. For iron ions with higher charge ($q = 23$–26), the $2s$ level is vacant as well, and electrons with angular momentum $l = 1$ may also decay to the ground state. In high-energy collisions, angular quantum numbers are populated in a statistical fashion, and the probability that the captured electron can radiatively decay via an $n_c \rightarrow n = 2$ transition is small. An electron in level n_c typically decays by a series of Yrast transitions, in which the angular momentum value in each step decreases by one unit. In the final step of this scenario, an X-ray is given off in the $n = 3 \rightarrow n = 2$ decay. However, if the collision energy is small (typically less than 1 keV amu^{-1}, as is the case in thermal plasmas), lower angular momentum values are preferentially populated, and the probability of $n_c \rightarrow n = 2$ and $n \geq 4 \rightarrow n = 2$ transitions increases strongly. This has been shown in the case of K-shell ions experimentally and theoretically (Beiersdorfer et al. 2000a; Perez et al. 2001). An increase in the hardness ratio was also observed by Tawara et al. (2003) in the case of energetic collisions ($\geq$3 keV amu^{-1}) of highly charged krypton ions with neutral gases. This preferential population of low angular momentum levels in low-energy charge-changing collisions is thus the basis for the significant differences found in the spectral shape when comparing spectra excited by charge exchange with spectra formed by electron-impact excitation.

As our measurements illustrate, even low-resolution spectra, such as those afforded by our solid-state detector, contain enough information to identify the signature of charge exchange. Higher resolution measurements, for example, those carried out with microcalorimeters (Beiersdorfer et al. 2003b; Porter et al. 2004; Chen et al. 2002, 2005), should provide the details necessary to identify which transitions contribute to the enhancement of the emission from $n = 4$ and 5. Detailed radiative cascade models may thus be able to discern whether these lines are, for example, preferentially populated by single-electron capture into high-n levels followed by cascades into the $n = 4$ and 5 levels, or by multielectron capture directly into the $n = 4$ and 5 levels.

Finally, we note that the observed enhancement of the iron L-shell emission due to excitation by charge exchange follows a pattern that is different from that observed in earlier measurements of the K-shell X-ray emission from hydrogen-like and helium-like ions. In the case of hydrogen-like ions, charge exchange resulted in strong flux from the level n_c that captured the electron. This resulted in a significant increase of the average energy of the X-rays emitted from hydrogen-like ions during charge exchange compared to line formation by electron-impact excitation. By contrast, the K-shell emission from helium-like ions showed no such enhancement. In fact, the emission of higher energy X-rays appears perhaps even suppressed when excited by charge exchange compared to electron-impact excitation. This is presumably because most charge exchange capture proceeds into triplet configurations, as predicated by statistical arguments, which are forbidden to decay to the $^1S_0$ helium-like ground state via X-ray emission. No such blocking of the decay paths exists in hydrogen-like ions. The behavior of the L-shell X-rays produced by charge

exchange seems to fall somewhere in between the extremes set by the K-shell emission from hydrogen-like and helium-like ions. Unlike the K-shell emission of helium-like ions, a clear enhancement was seen. However, unlike the K-shell emission of hydrogen-like ions, the enhanced flux is not near n_c, but most of the enhanced flux is seen in the emission from levels with $n = 4$ and $n = 5$.

Work at the University of California Lawrence Livermore National Laboratory was performed under the auspices of the Department of Energy under contract W-7405-Eng-48. P. L. and L. S. thank the German Academic Exchange Service DAAD for its support. This work was supported by NASA's Planetary Atmospheres Program under grant NNG 06-GB11G.

REFERENCES

Ali, R., Cocke, C. L., Raphaelian, M. L. A., & Stockli, M. 1994, Phys. Rev. A, 49, 3586
Ali, R., Neill, P. A., Beiersdorfer, P., Harris, C. L., Raković, M. J., Wang, J. G., Schultz, D. R., & Stancil, P. C. 2005, ApJ, 629, L125
Beiersdorfer, P. 2003, ARA&A, 41, 343
Beiersdorfer, P., Beck, B., Becker, S., & Schweikhard, L. 1996a, Int. J. Mass Spectrom. Ion Proc., 158, 149
Beiersdorfer, P., Becker, S., Beck, B., Elliott, S., Widmann, K., & Schweikhard, L. 1995a, Nucl. Instrum. Methods Phys. Res. B, 98, 558
Beiersdorfer, P., Bitter, M., Marion, M., & Olson, R. E. 2005a, Phys. Rev. A, 72, 032725
Beiersdorfer, P., Bitter, M., von Goeler, S., & Hill, K. W. 2004, ApJ, 610, 616
Beiersdorfer, P., Boyce, K. R., Brown, G. V., Chen, H., Kelley, R. L., Kilbourne, C. A., & Porter, F. S. 2005b, AGU Abstr. Spring, P42A-04
Beiersdorfer, P., Chen, H., Boyce, K. R., Brown, G. V., Kelley, R. L., Kilbourne, C. A., Porter, F. S., & Kahn, S. M. 2005c, Nucl. Instrum. Methods Phys. Res. B, 235, 116
Beiersdorfer, P., Decaux, V., Elliott, S., Widmann, K., & Wong, K. 1995b, Rev. Sci. Instrum., 66, 303
Beiersdorfer, P., Decaux, V., & Widmann, K. 1995c, Nucl. Instrum. Methods Phys. Res. B, 98, 566
Beiersdorfer, P., Lisse, C. M., Olson, R. E., Brown, G. V., & Chen, H. 2001, ApJ, 549, L147
Beiersdorfer, P., Osterheld, A. L., Decaux, V., & Widmann, K. 1996b, Phys. Rev. Lett., 77, 5353
Beiersdorfer, P., Schweikhard, L., Crespo López-Urrutia, J., & Widmann, K. 1996c, Rev. Sci. Instrum., 67, 3818
Beiersdorfer, P., Träbert, E., & Pinnington, E. H. 2003a, ApJ, 587, 836
Beiersdorfer, P., et al. 2000a, Phys. Rev. Lett., 85, 5090
———. 2000b, RevMexAA Ser. Conf., 9, 123
———. 2003b, Science, 300, 1558
Bhardwaj, A., et al. 2007, Planet. Space Sci., 55, 1135
Bliek, F. W., Woestenenk, G. R., Morgenstern, R., & Hoekstra, R. 1998, Phys. Rev. A, 57, 221
Brown, G. V., Beiersdorfer, P., Liedahl, D. A., Widmann, K., Kahn, S. M., & Clothiaux, E. J. 2002, ApJS, 140, 589
Brown, I. G., Galvin, J. E., MacGill, R. A., & Wright, R. T. 1986, Appl. Phys. Lett., 49, 1019
Chen, H., Gu, M. F., Behar, E., Brown, G. V., Kahn, S. M., & Beiersdorfer, P. 2007, ApJS, 168, 319
Chen, H., et al. 2005, ApJ, 618, 1086
———. 2002, ApJ, 567, L169
Cravens, T. E. 2002, Science, 296, 1042
Cravens, T. E., Waite, J. H., Gombosi, T. I., Lugaz, N., Gladstone, G. R., Mauk, B. H., & MacDowall, R. J. 2003, J. Geophys. Res. Space Physics, 108, 1465
Crespo López-Urrutia, J. R., Beiersdorfer, P., Savin, D. W., & Widmann, K. 1998, Phys. Rev. A, 58, 238
Dennerl, K., Englhauser, J., & Trümper, J. 1997, Science, 277, 1625
Dennerl, K., et al. 2006, A&A, 451, 709
Ehrenreich, T., et al. 2005, in AIP COnf. Proc. 774, X-Ray Diagnostics of Astrophysical Plasmas: Theory, Experiment, and Observation , ed. R. Smith (New York: AIP), 281
Elsner, R. F., et al. 2005, J. Geophys. Res. Space Phys., 110, 1207
Gladstone, G. R., et al. 2002, Nature, 415, 1000
Greenwood, J. B., Williams, I. D., Smith, S. J., & Chutjian, A. 2000, ApJ, 533, L175
———. 2001, Phys. Rev. A, 63, 062707
Häberli, R. M., Gombosi, T. I., Zeeuw, D. L. D., Combi, M. R., & Powell, K. G. 1997, Science, 276, 939
Hasan, A. A., Eissa, F., Ali, R., Schultz, D. R., & Stancil, P. C. 2001, ApJ, 560, L201
Ip, W.-H., & Chow, V. W. 1997, Icarus, 130, 217
Janev, R. K., & Winter, H. 1985, Phys. Rep., 117, 265
Kelly, R. L. 1987, J. Phys. Chem. Ref. Data, 16, Suppl. 1
Kharchenko, V., & Dalgarno, A. 2001, ApJ, 554, L99
Kharchenko, V., Rigazio, M., Dalgarno, A., & Krasnopolsky, V. A. 2003, ApJ, 585, L73
Krasnopolsky, V. A. 1997, Icarus, 128, 368
Krasnopolsky, V. A., Christian, D. J., Kharchenko, V., Dalgarno, A., Wolk, S. J., Lisse, C. M., & Stern, S. A. 2002, Icarus, 160, 437
Krasnopolsky, V. A., Mumma, M. J., Abbott, M., Flynn, B. C., Meech, K. J., Yeomans, D. K., Feldmann, P. D., & Cosmovici, C. B. 1997, Science, 277, 1488
Lapierre, A., et al. 2005, Phys. Rev. Lett., 95, 183001
Liebisch, P. 1998, Dimplomarbeit, Humboldt Universität
Lisse, C. M., Christian, D. J., Dennerl, K., Meech, K. J., R. Petre, H. A. W., & Wolk, S. J. 2001, Science, 292, 1343
Lisse, C. M., et al. 1996, Science, 274, 205
———. 1999a, Earth, Moon, Planets, 77, 283
———. 1999b, Icarus, 141, 316
———. 2005, ApJ, 635, 1329
Lubinski, G., Juhász, Z., Morgenstern, R., & Hoekstra, R. 2000, J. Phys. B, 33, 5275
Major, F. G., Gheorghe, V. N., & Werth, G. 2004, Charged Particle Traps (Berlin: Springer)
Mumma, M. J., Krasnopolsky, V. A., & Abbott, M. J. 1997, ApJ, 491, L125
Neill, P., Beiersdorfer, P., Brown, G., Harris, C., Träbert, E., Utter, S. B., & Wong, K. L. 2000, Phys. Rev. A, 62, 141
Neugebauer, M., Cravens, T. E., Lisse, C. M., Ipavich, F. M., von Steiger, R., Shah, P. D., & Armstrong, T. P. 2000, J. Geophys. Res., 105, 20949
Otranto, S., Olson, R. E., & Beiersdorfer, P. 2006, Phys. Rev. A, 73, 022723
Perez, J. A., Olson, R. E., & Beiersdorfer, P. 2001, J. Phys. B, 34, 3063
Porter, F. S., et al. 2004, Rev. Sci. Instrum., 75, 3772
Schwadron, N. A., & Cravens, T. E. 2000, ApJ, 544, 558
Schweikhard, L., Beiersdorfer, P., Brown, G. V., Crespo López-Urrutia, J. R., Utter, S. B., & Widmann, K. 1998, Nucl. Instrum. Methods Phys. Res. B, 142, 245
Schweikhard, L., Beiersdorfer, P., & Träbert, E. 2002, in AIP Conf. Proc. 606, Non-Neutral Plasma Phys. IV, ed. F. Anderegg et al. (New York: AIP), 174
Schweikhard, L., Ziegler, J., Beiersdorfer, P., B. Beck, S. B., & Elliott, S. 1995, Rev. Sci. Instrum., 66, 448
Tawara, H., Richard, P., Safronova, U. I., Vasilyev, A. A., & Hansen, S. 2002, Phys. Rev. A, 65, 042509
Tawara, H., Takacs, E., Ratcliff, L. P., Gillaspy, J. D., & Tökesi, K. 2003, Nucl. Instrum. Methods Phys. Res. B, 205, 605
Träbert, E., Beiersdorfer, P., Brown, G. V., Chen, H., Pinnington, E. H., & Thorn, D. B. 2001, Phys. Rev. A, 64, 034501
Träbert, E., Beiersdorfer, P., Gwinner, G., Pinnington, E. H., & Wolf, A. 2002, Phys. Rev. A, 66, 052507
Träbert, E., et al. 2000, ApJ, 541, 506
Wargelin, B. J., Beiersdorfer, P., Neill, P. A., Olson, R. E., & Scofield, J. H. 2005, ApJ, 634, 687
Wargelin, B. J., & Drake, J. J. 2002, ApJ, 578, 503
Wargelin, B. J., Kahn, S. M., & Beiersdorfer, P. 2001, Phys. Rev. A, 63, 022710
Wargelin, B. J., Markevitch, M., Juda, M., Kharchenko, V., Edgar, R., & Dalgarno, A. 2004, ApJ, 607, 596
Wegmann, R., Schmidt, H. U., Lisse, C. M., Dennerl, K., & Englhauser, J. 1998, Planet. Space Sci., 46, 603
Wise, M. W., & Sarazin, C. L. 1989, ApJ, 345, 384